

Feeding activates FGF15-SHP-TFEB-mediated lipophagy in the gut

Sunmi Seok¹, Young-Chae Kim^{1,†,‡}, Yang Zhang^{2,†} , Bo Kong³ , Grace Guo³, Jian Ma² , Byron Kemper¹ & Jongsook Kim Kemper^{1,*} 

Abstract

Lysosome-mediated macroautophagy, including lipophagy, is activated under nutrient deprivation but is repressed after feeding. We show that, unexpectedly, feeding activates intestinal autophagy/lipophagy in a manner dependent on both the orphan nuclear receptor, small heterodimer partner (SHP/NROB2), and the gut hormone, fibroblast growth factor-15/19 (FGF15/19). Furthermore, postprandial intestinal triglycerides (TGs) and apolipoprotein-B48 (ApoB48), the TG-rich chylomicron marker, were elevated in SHP-knockout and FGF15-knockout mice. Genomic analyses of the mouse intestine indicated that SHP partners with the key lysosomal activator, transcription factor-EB (TFEB) to upregulate the transcription of autophagy/lipolysis network genes after feeding. FGF19 treatment activated lipophagy, reducing TG and ApoB48 levels in HT29 intestinal cells, which was dependent on TFEB. Mechanistically, feeding-induced FGF15/19 signaling increased the nuclear localization of TFEB and SHP via PKC beta/zeta-mediated phosphorylation, leading to increased transcription of the TFEB/SHP target lipophagy genes, Ulk1 and Atg1. Collectively, these results demonstrate that paradoxically after feeding, FGF15/19-activated SHP and TFEB activate gut lipophagy, limiting postprandial TGs. As excess postprandial lipids cause dyslipidemia and obesity, the FGF15/19-SHP-TFEB axis that reduces intestinal TGs via lipophagic activation provides promising therapeutic targets for obesity-associated metabolic disease.

Keywords ATGL; autophagy; FGF19; SHP; TFEB

Subject Categories Autophagy & Cell Death

DOI 10.15252/embj.2021109997 | Received 20 October 2021 | Revised 19 April 2022 | Accepted 21 April 2022 | Published online 10 June 2022

The EMBO Journal (2022) 41: e109997

See also: [N Raimundo](#) (September 2022)

Introduction

Lysosome-mediated macroautophagy is a highly conserved catabolic process that recycles diverse cytoplasmic materials for cellular

survival and homeostasis under nutrient deprivation (Kuma *et al*, 2004; Levine & Klionsky, 2004; Morishita & Mizushima, 2019). Since its discovery (Singh *et al*, 2009), autophagic degradation of cytosolic lipid droplets, lipophagy, has been shown to be critical for the maintenance of energy balance during starvation (Martinez-Lopez & Singh, 2015; Schulze *et al*, 2017; Zechner *et al*, 2017; Kounakis *et al*, 2019). Although the acute post-translational regulation of pre-existing autophagy machinery by nutrient-sensing kinases, such as mTOR and AMPK, has been studied extensively (He & Klionsky, 2009), longer-term transcription regulation has emerged as a major mechanism for sustained autophagic control in response to nutrient availability (Fullgrave *et al*, 2014; Settembre & Ballabio, 2014; Baek & Kim, 2017; Di Malta *et al*, 2019).

A growing body of recent studies has linked transcription regulation of autophagy with lipid metabolism in mouse liver. For instance, transcription factor-EB (TFEB), a master activator of lysosomal biogenesis, promotes lipid catabolism via autophagic activation during fasting (Settembre *et al*, 2011, 2013). Under nutrient deprivation, JMJD3 histone demethylase, together with PPAR α and SIRT1, increases TFEB gene expression, transcriptionally activating lipophagy in response to the fasting-induced hepatokine, FGF21 (Seok *et al*, 2018; Byun *et al*, 2020). In contrast, the bile acid nuclear receptor, farnesoid-X-receptor (FXR/NR1H4), mediates transcription repression of autophagy network genes after feeding, via inhibition of the autophagic activators, CREB and PPAR α (Lee *et al*, 2014; Seok *et al*, 2014). Well-known targets of FXR, the nuclear receptor, small heterodimer partner (SHP/NROB2), and the gut hormone, fibroblast growth factor-15/19 (human FGF19, mouse FGF15) (Kliwer & Mangelsdorf, 2015; Gadaleta & Moschetta, 2019), further sustain the repression in the late fed-state (Byun *et al*, 2017).

Small heterodimer partner is an unusual orphan nuclear receptor that does not contain a DNA binding domain and normally acts as a corepressor (Seol *et al*, 1996). SHP inhibits the activity of numerous transcription factors involved in diverse biological pathways, including LRH-1, AHR, SREBPs, and p53 (Lee & Moore, 2002; Lee *et al*, 2010; Kim *et al*, 2015, 2018b). SHP is best known for its inhibition of hepatic bile acid synthesis (Kerr *et al*, 2002; Wang *et al*, 2002), but recent genomic studies in mouse liver revealed new

1 Department of Molecular and Integrative Physiology, University of Illinois at Urbana-Champaign, Urbana, IL, USA

2 Computational Biology Department, School of Computer Science, Carnegie Mellon University, Pittsburgh, PA, USA

3 Department of Pharmacology and Toxicology, Ernest Mario School of Pharmacy, Rutgers University, Piscataway, NJ, USA

*Corresponding author. Tel: +1 217 333 6317; E-mail: jongsook@illinois.edu

†These authors contributed equally to this work

‡Present address: Cardiovascular Branch, National Heart, Lung, and Blood Institute, National Institutes of Health, Bethesda, MD, USA

physiological functions in lipogenesis, cholesterol synthesis and the one carbon cycle in response to feeding-induced FGF15/19 (Kim *et al.*, 2015, 2018b, 2020). After feeding, FGF15/19-activated SHP also represses autophagy network genes in mouse liver (Byun *et al.*, 2017), but it is not known whether SHP regulates autophagy in other metabolic tissues, such as intestines.

The intestine plays a crucial role in the maintenance of whole-body lipid homeostasis. After a meal, dietary lipids, triglycerides (TG), are digested and absorbed into enterocytes as free fatty acids. After being re-synthesized, TGs are packaged into chylomicron particles, and the postprandial lipids are distributed via TG-rich chylomicrons to the liver and other tissues (Hussain, 2014). This postprandial process must be tightly regulated as elevated postprandial lipids can lead to dyslipidemia and obesity (Hodson & Gunn, 2019). However, how intestinal TG levels are regulated during feeding/fasting cycles is poorly understood.

In this study, we show that surprisingly, feeding activates intestinal lipophagy in mice, in a manner dependent on both SHP and FGF15/19, regulating postprandial TG levels for secretion. With genomic analyses and mechanistic studies, we further show that feeding-induced FGF15/19 signaling activates both SHP and the key autophagic activator TFEB by increasing their nuclear localization via PKC-mediated phosphorylation, leading to transcription induction of the TFEB/SHP targets, *Ulk1* and *Atgl*, which are essential for lipophagy.

Results

Feeding inhibits hepatic autophagy but paradoxically activates intestinal autophagy

Autophagy is activated during fasting and repressed after feeding in mouse liver (Lee *et al.*, 2014; Seok *et al.*, 2014; Byun *et al.*, 2017, 2020). To determine whether nutrient regulation of autophagy occurs in mouse intestine under physiological conditions, we examined the effects of fasting and refeeding on autophagic markers: the ratio of lipidated LC3-II to non-lipidated LC3-I and the levels of p62/SQSTM1, the autophagosome adaptor, and LAMP1, a lysosomal membrane protein (Klionsky *et al.*, 2021), in both intestinal and liver extracts. In liver extracts of C57BL/6 mice, feeding decreased the LC3-II/I ratio and LAMP1 levels, and increased p62 levels, indicative of the repression of autophagy (Fig 1A). Surprisingly, the opposite response to feeding was observed in intestinal extracts from the same mice (Fig 1A). These results indicate that after feeding, autophagy is inhibited in the liver at the same time it is activated in the intestine.

Feeding activation of intestinal autophagy is dependent on both SHP and FGF15

FGF15/19 is a late fed-state gut hormone that ensures a smooth metabolic transition between feeding and fasting to maintain bile acid and lipid homeostasis (Kliewer & Mangelsdorf, 2015; Byun *et al.*, 2018; Gadaleta & Moschetta, 2019; Kim *et al.*, 2020). As FGF15/19-activated SHP inhibits hepatic autophagy (Byun *et al.*, 2017), we further examined the role of SHP and FGF15 in the feeding activation of intestinal autophagy. The increased intestinal LC3-II/I ratio and LAMP1 levels and decreased p62 levels observed in control mice after feeding were largely absent in both SHP-knockout

(KO) and FGF15-KO mice (Fig 1B and C). Consistent with these results, expression of LC3, a marker protein for autophagosome detected by immunohistochemistry (IHC), was increased after feeding in control mice, but the increase was substantially reduced in SHP-KO and FGF15-KO mice (Fig 1D and E). These results demonstrate that feeding inhibits autophagy in the liver but activates it in the intestine, and that feeding induction of intestinal autophagy is dependent on both SHP and FGF15.

The feeding-sensing nuclear receptor, FXR, mediates transcription repression of hepatic autophagy after feeding (Lee *et al.*, 2014; Seok *et al.*, 2014). Consistent with the gene induction of both *Shp* and *Fgf15* by FXR (Kliewer & Mangelsdorf, 2015), feeding activation of gut autophagy was largely abolished in FXR-KO mice (Appendix Fig S1). These results suggest that FXR is also important for feeding induction of intestinal autophagy.

Identification of genome-wide intestinal SHP binding sites in mice

To investigate the mechanisms by which SHP and FGF15/19 activate intestinal autophagy after feeding, we identified the SHP cistrome in mouse intestine by ChIP-seq analysis. As protein stability and nuclear localization of SHP are increased in the late fed-state via FGF15/19 signaling (Miao *et al.*, 2009; Seok *et al.*, 2013; Kim *et al.*, 2018b, 2020), we performed intestinal ChIP-seq analysis of SHP binding in mice after feeding.

In the C57BL/6 mice, 5,700 SHP binding peaks at 5,200 genes were identified and SHP binding sites were located most frequently near TSS, but also were detected in 5'-UTRs, introns, and exons (Appendix Fig S2). Analysis of published intestinal RNA-seq data (Kim *et al.*, 2018a) revealed that about equal numbers of genes were up or downregulated in fed SHP-KO mice compared with C57BL/6 mice (Appendix Fig S3), suggesting that SHP, either directly or indirectly, both activates and inhibits intestinal genes.

SHP is a potential global activator of intestinal autophagy, catabolism, and circadian genes

Genes that have both SHP binding sites and altered expression in SHP-KO mice are most likely directly regulated by SHP. In comparative genomic analysis of the intestinal SHP cistrome (Appendix Figs S2 and S3) with transcriptome data (Kim *et al.*, 2018a), expression was significantly decreased in SHP-KO mice for 856 genes (Appendix Table S1) of the 5,200 genes with SHP binding sites (Fig 2A), suggesting that these genes may be directly activated by SHP binding.

Gene ontology (G/O) analysis of the 856 genes suggested that SHP upregulates genes involved in autophagy, catabolic processes, and the circadian rhythm (Fig 2B) and in heat map analysis, genes involved in these biological processes were downregulated in SHP-KO mice (Fig 2C). SHP binding peaks at selected key genes involved in autophagy (*Ulk1* and *Wipi2*), lipolysis (*Atgl* and *Ppar α*), and diurnal regulation (*Nampt* and *Bmal1*) are illustrated in Fig 2D. SHP binding was confirmed by ChIP with two different SHP antibodies (Fig 2E, Appendix Fig S4A), and the expression of the genes was decreased in SHP-KO mice compared with WT mice (Fig 2F). These genomic analyses are consistent with the results above that feeding activation of gut autophagy is dependent on SHP (Fig 1) and further suggest an unexpected activation function of SHP in intestinal autophagy, lipid catabolism, and circadian genes.

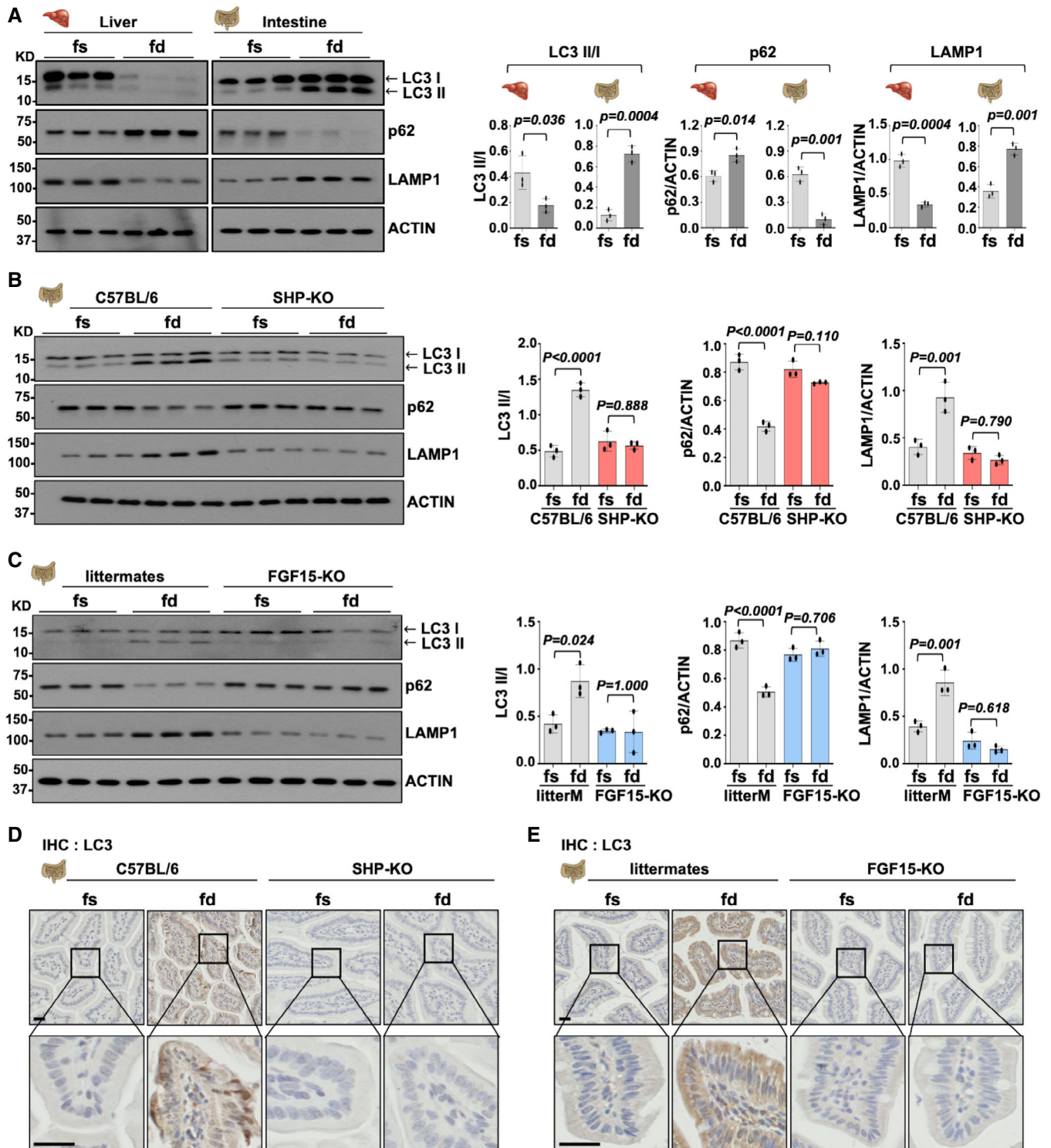


Figure 1. Paradoxical feeding activation of gut autophagy is dependent on both SHP and FGF15.

C57BL/6, SHP-KO, and FGF15-KO or littermate mice were fasted overnight and then re-fed for 6 h.

A–C Levels of the indicated proteins detected by IB in (A) liver and intestinal extracts from C57BL/6 mice and in intestinal extracts from (B) C57BL/6 or SHP-KO mice or (C) FGF15-KO mice or littermates. Band quantitation was done using Image J, and the LC3 II/I ratio and p62/actin and lamp1/actin ratios are shown at the right.

D, E Endogenous LC3 was detected by IHC in intestinal sections from (D) SHP-KO and C57BL/6 mice or (E) FGF15-KO mice and littermates. Scale bar, 20 μ m.

Data information: (A–C) The mean and standard deviation (SD) are plotted. Statistical significance was determined by (A) two-tailed Student's *t*-tests or (B, C) two-way ANOVA with the Tukey post-test. *P*-values are indicated (*n* = 3 mice).

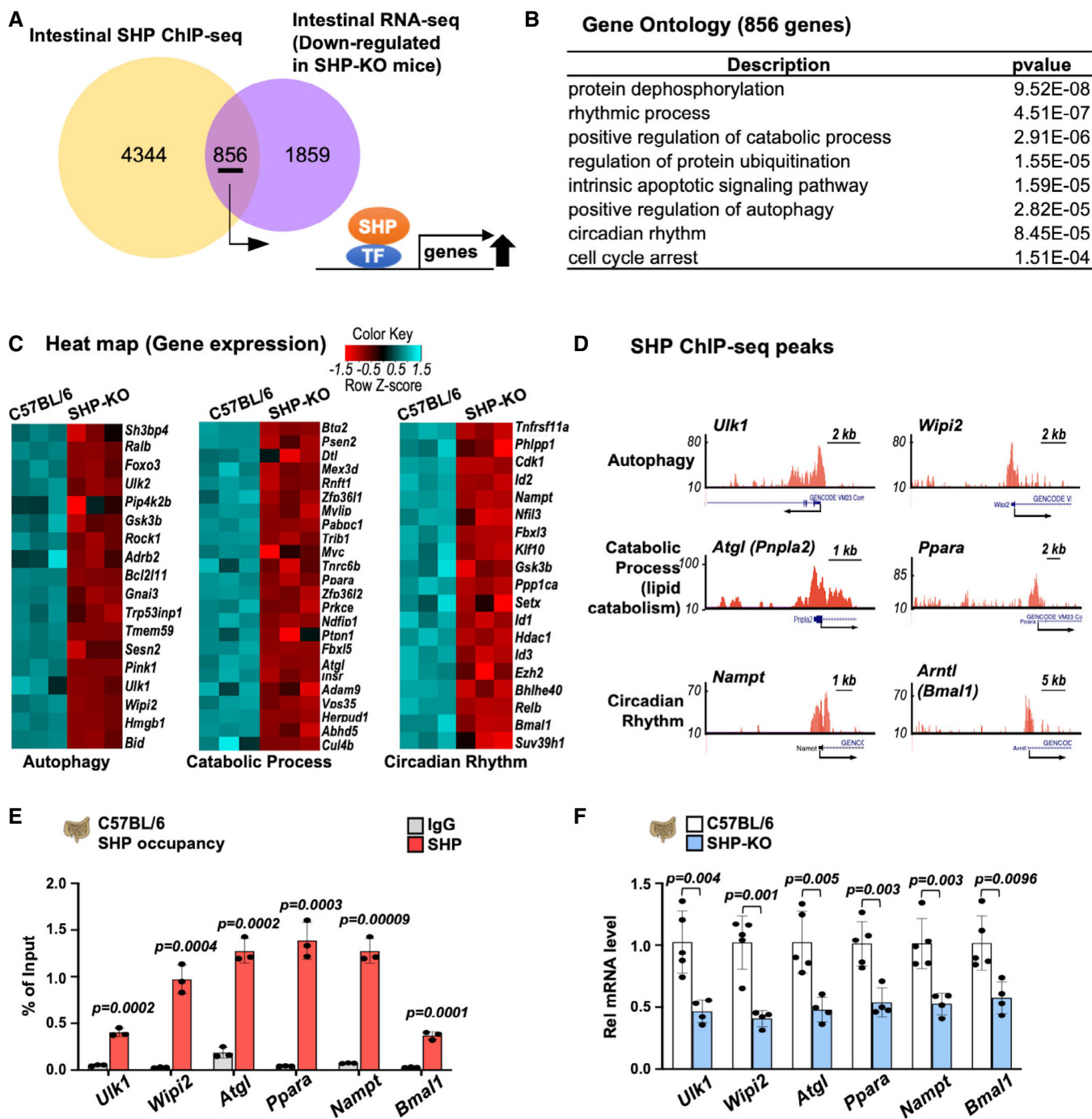


Figure 2. SHP is a potential global activator of intestinal autophagy, lipid catabolism, and circadian genes.

A Venn diagram showing the genes with SHP binding peaks in intestine from C57BL/6 mice (yellow) after refeeding for 4 h and downregulated intestinal genes in SHP-KO mice (purple) after refeeding for 6 h.

B GO analysis of the 856 intestinal genes with SHP binding peaks that are downregulated in SHP-KO mice.

C Heat map from the intestinal RNA-seq data comparing expression of the indicated genes in C57BL/6 and SHP-KO mice. Independent analyses were done for three mice in each group.

D UCSC Genome Browser display showing SHP binding peaks at the indicated intestinal genes.

E Occupancy of SHP at the indicated intestinal genes determined by CHIP ($n = 3$ mice).

F Comparison of relative (C57BL/6 values set to 1) intestinal mRNA levels in C57BL/6 and SHP KO mice for the indicated genes determined by RT-qPCR ($n = 4-5$ mice).

Data information: (E, F) The mean and SD are plotted. Statistical significance was determined by the two-tailed Student's *t*-test and *P*-values are indicated.

SHP is a potential global repressor of intestinal lipid synthesis/absorption and bile acid recycling genes

For intestinal genes that were upregulated in the SHP-KO mice, 774 genes (Appendix Table S2) also had SHP binding sites (Fig 3A), suggesting that SHP directly inhibits these genes. Biological processes inhibited by SHP included lipid synthesis/absorption, membrane transport, and bile acid recycling (Fig 3B), and genes related to these processes, were upregulated in SHP-KO mice (Fig 3C). SHP binding peaks at genes involved in lipid absorption (*Cd36*, *Npc1l1*), lipid synthesis (*Dgat1*, *Acty*), and bile acid recycling (*Asbt*, *Nhe3*) are illustrated (Fig 3D) and SHP binding to these genes (Fig 3E, Appendix Fig S4B) and their increased expression in SHP-KO mice were confirmed (Fig 3F). These global analyses suggest that SHP represses lipid absorption/synthesis genes, which is consistent with recent studies that FGF19 and SHP inhibit *Npc1l1* and cholesterol absorption in mouse intestine (Kim et al, 2018a) and intestinal SHP is important for overall intestinal structure and bile acid homeostasis (Nguyen et al, 2021).

Postprandial intestinal TG and ApoB48 levels are elevated in SHP-KO and FGF15-KO mice

Our genomic analyses above suggested that after feeding, SHP directly upregulates intestinal autophagy and lipid catabolism genes (Fig 2), and conversely, downregulates lipid synthesis and absorption genes (Fig 3), which would be expected to decrease intestinal TG levels. We, therefore, examined the effects of fasting and refeeding on TG levels in WT and SHP-KO mice. Intestinal TG levels were increased after feeding in C57BL/6 mice and postprandial TG levels were elevated even higher in SHP-KO mice (Fig 4A).

Intestinal TG levels are a key determinant driving TG-rich chylomicron formation (Hussain, 2014). ApoB48 is a quantitative marker of intestinal chylomicrons, as it is specific to intestinal chylomicrons and each chylomicron particle contains one molecule of ApoB48 (Phillips et al, 1997). Consistent with increased TG levels, intestinal ApoB48 levels were elevated in SHP-KO mice (Fig 4B). Consistent with the role of FGF15 in activation of SHP in lipid regulation (Kim et al, 2018a, 2020) and feeding induction of gut autophagy (Fig 1), TG and ApoB48 levels were also increased in FGF15-KO mice after feeding (Fig 4C and D). In IHC analysis, intestinal expression of ApoB48 was mostly detected in enterocytes, although some was detected in epithelial cells, and increased after feeding in C57BL/6 mice, and the increase was elevated even higher in both SHP-KO and FGF15-KO mice (Fig 4E and F). These results, together with the autophagic studies in mice (Fig 1), suggest that both SHP and FGF15 are critical for reducing intestinal TG and ApoB48 levels after feeding in mice.

FGF19 promotes lipophagy in HT29 human intestinal cells

HT29 cells have been utilized to elucidate *in vitro* mechanisms of intestinal chylomicron biogenesis and bile acid/cholesterol regulation (Kim et al, 2018a; Zhang et al, 2019). To determine whether FGF15/19 and SHP promote intestinal lipophagy, we examined the co-localization of the autophagic marker LC3 with PLIN2, a marker for lipid droplets, by immunofluorescence in HT29 cells. Consistent with the role of FGF15/19 and SHP in reducing intestinal TGs levels in mice (Fig 4A–D), FGF19 treatment increased co-localization of LC3 puncta with PLIN2, indicating catabolism of lipid droplets by

lipophagy (Sathyanarayan et al, 2017; Tsai et al, 2017) (Fig 4G). The FGF19-mediated lipophagic activation was largely abolished by downregulation of SHP, whereas it was markedly enhanced by overexpression of SHP (Fig 4G). Moreover, FGF19 treatment increased the LC3 II/I ratio, and these effects were still observed after treatment with bafilomycin A1, a lysosomal inhibitor, suggesting that FGF19 increases the autophagic flux (Fig 4H). Furthermore, FGF19 treatment resulted in decreased ApoB48 levels and these FGF19 effects were blocked by downregulation of LAMP1, a lysosomal membrane protein (Fig 4I). These results, together, demonstrate that FGF19 activates intestinal lipophagy in a SHP-dependent manner in HT29 cells.

FGF19 promotes lipophagy, reducing TG and ApoB48 levels in HT29 cells

To further determine whether FGF19 reduces intestinal TG levels via lipophagic activation, we examined the effect of FGF19 combined with downregulation of the key autophagosome protein ATG7 (Appendix Fig S5A), on lipophagy and cellular TG/ApoB48 levels in HT29 cells. FGF19 treatment increased co-localization of LC3 puncta with PLIN2 and this FGF19-mediated lipophagic activation was abolished by downregulation of ATG7 (Fig 5A). These results were consistent with co-localization of LC3 puncta with BODIPY-stained lipids (Appendix Fig S5B). Consistent with lipophagic activation, FGF19 treatment increased the LC3-II/I ratio (Fig 5B) and decreased cellular TG/ApoB48 levels (Fig 5C and D). These FGF19 effects were substantially diminished in *Atg7*-downregulated autophagy-defective cells (Fig 5A–D), suggesting that FGF19-mediated lipid effects were dependent on lipophagic activation. These results, together, demonstrate that FGF19 reduces cellular TG and ApoB48 levels in part via lipophagic activation in HT29 cells.

Global motif analyses predict that SHP partners with TFEB in the induction of intestinal lipophagy network genes

We further investigated molecular mechanisms by which SHP directly activates expression of intestinal autophagy/lipolysis genes. As SHP does not contain a DNA binding domain, we performed a global motif analysis of SHP binding regions to identify transcription factors that could functionally interact with SHP.

For genes activated by SHP binding, the motifs detected included those for a circadian activator (*Bhlhe41*), for autophagic activators (TFEB and TFE3) (Settembre et al, 2013; Di Malta et al, 2019), and for an autophagic repressor (*ZKSCAN3*) (Chauhan et al, 2013) (Fig 6A, Appendix Table S4). For genes repressed by SHP binding, unique motifs detected included those for p53, ZEB1 and NRF1 (Fig 6A, Appendix Table S3). These results suggest that direct gene activation or repression by SHP binding involves different sets of transcription factors. Particularly for the upregulated genes, motifs for autophagic activators, such as TFEB, TFE3, support the genomic data that SHP directly activates autophagy genes (Fig 2).

Feeding induces the functional interaction between SHP and TFEB at *Ulk1* and *Atg1*

To elucidate the mechanism of feeding activation of intestinal lipophagy genes by SHP binding, we focused on TFEB, a key activator of lysosome and autophagy network genes (Settembre et al, 2011; Di Malta

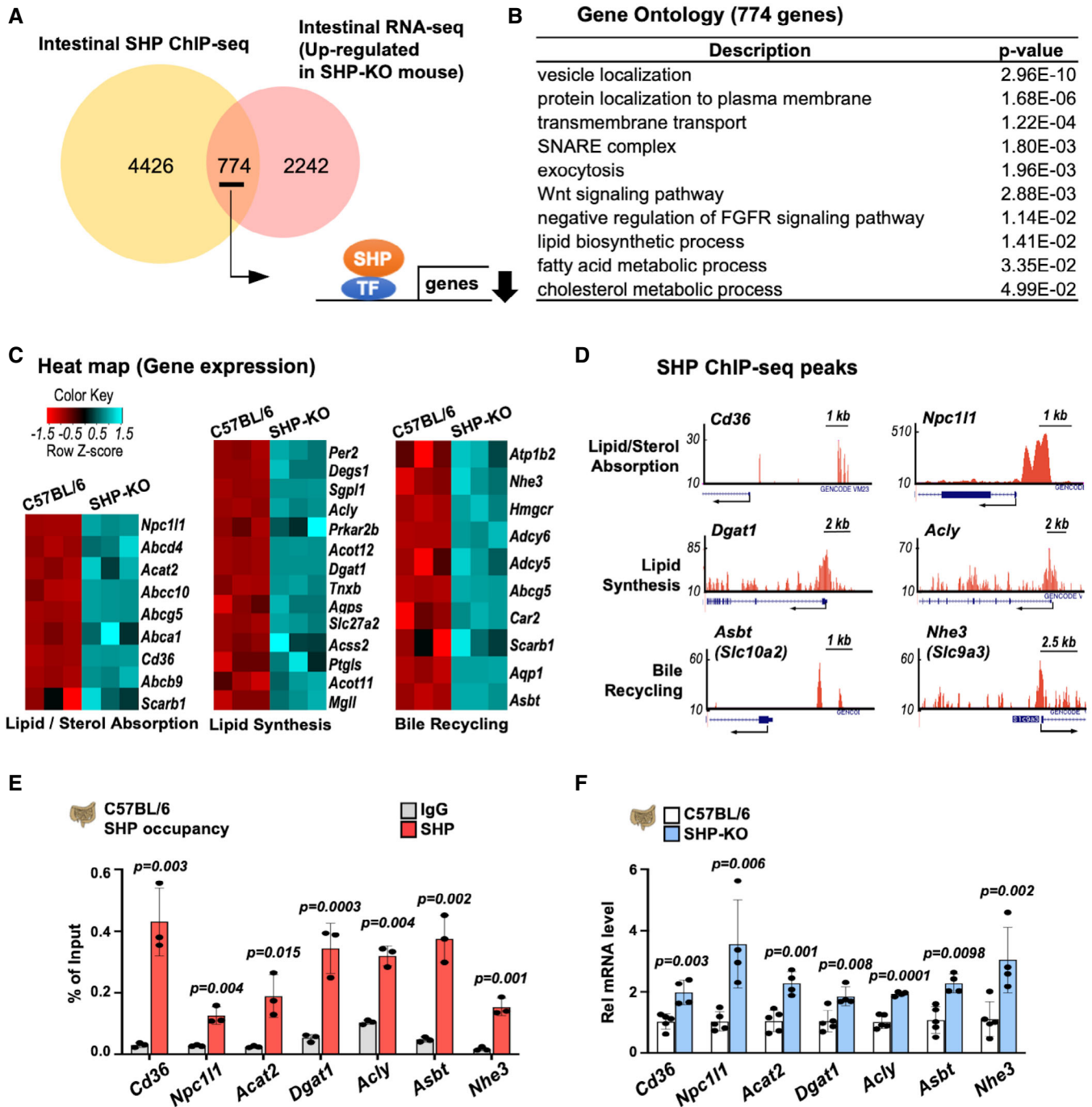


Figure 3. SHP is a potential global repressor of intestinal lipid absorption/synthesis and bile acid recycling genes.

A Venn diagram showing intestinal genes with SHP binding peaks in C57BL/6 mice (yellow) and those that are upregulated in SHP-KO mice (pink) after refeeding for 4 and 6 h, respectively.

B G/O analysis of the 774 intestinal genes with SHP binding peaks that are upregulated in SHP-KO mice.

C Heat map comparing expression of the indicated intestinal genes in three C57BL/6 or SHP-KO mice. Independent analyses were done for three mice in each group.

D UCSC Genome Browser display showing SHP binding peaks at the indicated intestinal genes.

E Occupancy of SHP at the indicated genes determined by ChIP (n = 3 mice).

F Comparison of relative (C57BL/6 values set to 1) intestinal mRNA levels in C57BL/6 and SHP-KO mice for the indicated genes by RT-qPCR (n = 4–5 mice).

Data information: (E, F) The mean and SD are plotted. Statistical significance was determined by two-tailed Student's t-tests. P-values are indicated.

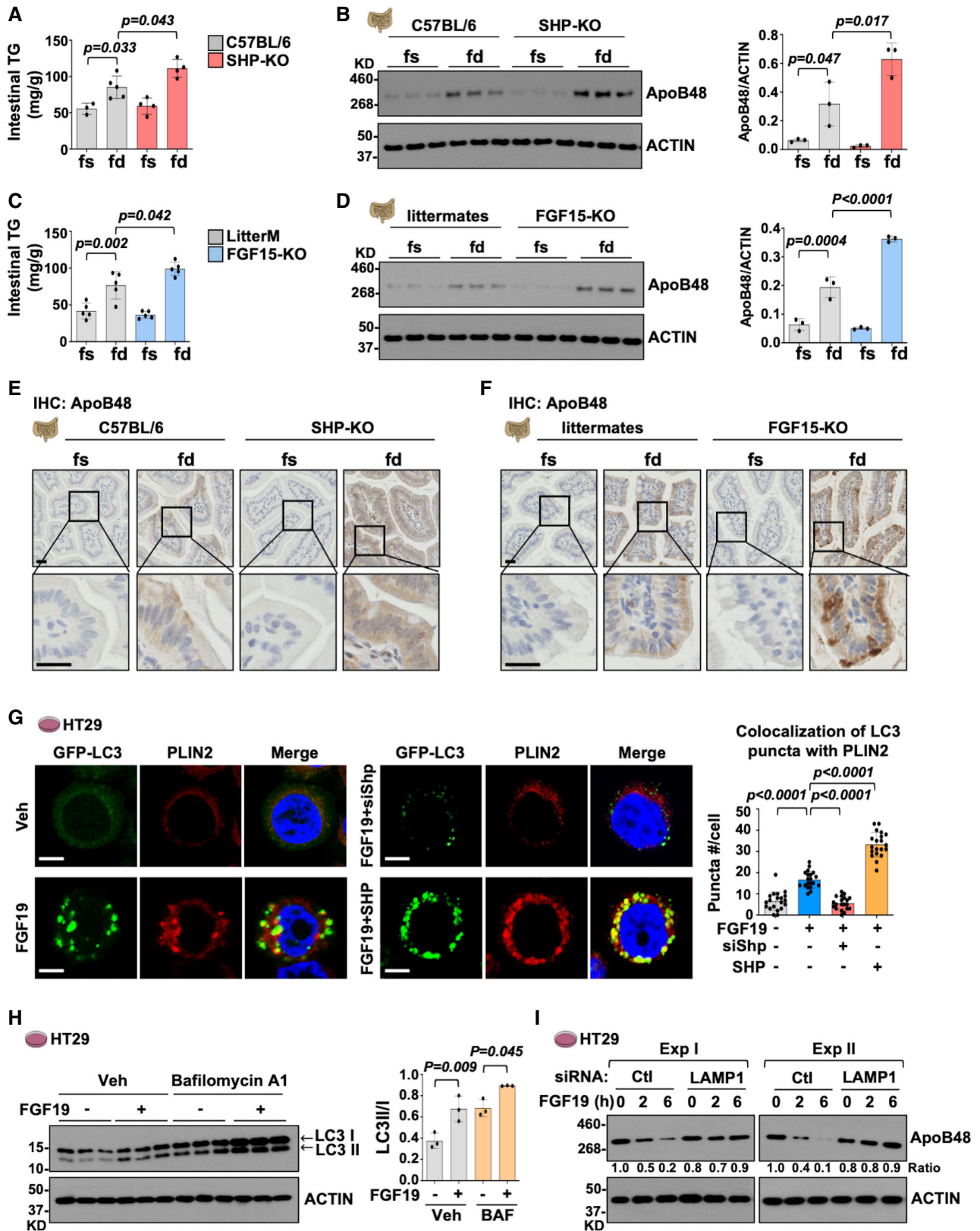


Figure 4.

Figure 4. Feeding-mediated increases in intestinal TG and ApoB48 levels are enhanced in SHP-KO and FGF15-KO mice.

- A–F C57BL/6, SHP-KO, and FGF15-KO or littermate mice as indicated were fasted for 12 h and then, re-fed for 6 h. (A–D) Intestinal TG levels in (A) C57BL/6 and SHP-KO mice or (C) FGF15-KO mice and littermates and levels of the indicated proteins in intestinal extracts from (B) C57BL/6 and SHP-KO mice or (D) FGF15-KO mice and littermates with quantitation of the bands at right. (A, C) $n = 3–5$ mice, (B, D) $n = 3$ mice. (E, F) Endogenous ApoB48 levels were detected by IHC in intestinal sections of SHP-KO and C57BL/6 mice (E) or FGF15-KO mice and littermates (F). Scale bar, 20 μm .
- G HT29 cells were transfected with GFP-LC3 and with SHP siRNA or SHP expression plasmids and incubated in serum-free medium containing 200 μM oleic acid for 6 h followed by treatment with 50 ng/ml FGF19 for 6 h as described in Materials and Methods. The control group (Veh) was treated with vehicle for FGF19, control plasmid DNA, and scrambled siRNA. The FGF19 groups were treated with control DNA or SHP expression plasmid or SHP siRNA or control scrambled siRNA as indicated. Cells were imaged by confocal microscopy (Zeiss, LSM700). GFP-LC3 puncta were counted and the number of puncta/cell is shown at right ($n = 20$). Scale bar, 10 μm .
- H HT29 cells were treated with 50 ng/ml FGF19 with or without 100 nM bafilomycin A1 for 12 h. LC3 and actin levels in cell extracts were determined by IB. Quantification of bands is shown at the right ($n = 3$ culture plates).
- I HT29 cells were transfected with *Lamp1* siRNA or scrambled siRNA and 48 h later were treated with 50 ng/ml FGF19 for the indicated times. ApoB48 and actin levels were determined by IB ($n = 2$ culture plates).

Data information: (A–D, G, H) The mean and SD are plotted. Statistical significance was determined by (A–D, H) two-way ANOVA with the Tukey post-test or (G) one-way ANOVA with the Tukey post-test. P -values are indicated, (A, C) $n = 3–5$ mice, (B, D) $n = 3$ mice.

et al, 2019), First, in CoIP studies in intestinal extracts, feeding increased the interaction between SHP and TFEB in littermates but not in FGF15-KO mice (Fig 6B), suggesting that endogenous FGF15 signaling after feeding is likely important for the SHP-TFEB interaction.

ULK1 is the autophagy-initiating kinase (He & Klionsky, 2009) and ATGL is an essential protein for lipophagy (Schulze *et al*, 2017; Zechner *et al*, 2017; Kounakis *et al*, 2019). ATGL has been demonstrated to be both necessary and sufficient for lipophagy induction in mice (Sathyanarayan *et al*, 2017). As *Ulk1* and *Atgl* are direct target genes of SHP in genomic analyses (Fig 2D–F), we examined the transcriptional regulation of both genes. First, we tested whether the occupancy of TFEB and SHP at *Ulk1* and *Atgl* genes is increased after feeding. In ChIP assays in mouse intestine, feeding substantially increased the occupancy of both TFEB and SHP at *Ulk1* and *Atgl* (Fig 6C). Feeding also increased the occupancy of RNA pol II, an indicator of gene activation, at both genes (Fig 6C). In re-ChIP assays, feeding increased SHP occupancy in TFEB-bound chromatin at *Ulk1* and *Atgl* (Fig 6D), suggesting that feeding induces the TFEB interaction with SHP at these genes. These results, together, indicate that feeding increases the functional interaction between SHP and TFEB at *Ulk1* and *Atgl*, resulting in transcription induction of the genes.

We further examined functional interactions between TFEB and SHP in the induction of *Ulk1* in HT29 cells. In luciferase reporter assays, exogenous expression of TFEB increased transactivation of the *Ulk1* promoter and overexpression of SHP enhanced the TFEB-mediated transactivation in a largely FGF19-dependent manner since little transactivation was observed without FGF19 treatment (Fig 6E). In contrast, downregulation of SHP inhibited the TFEB transactivation of the *Ulk1*-reporter and conversely, downregulation of TFEB blocked the SHP transactivation of the reporter activity. These results indicate that SHP enhances the TFEB-mediated transactivation of *Ulk1*. Consistent with these findings, protein levels of ULK1 and ATGL in intestinal extracts were increased after feeding in WT mice, but the increase was absent in both SHP-KO and FGF15-KO mice (Fig 6F and G), demonstrating that feeding induction of ULK1 and ATGL is dependent on SHP and FGF15.

TFEB is critical for FGF19-mediated lipophagy and lipid-lowering effects in HT29 cells

The global motif analysis and biochemical studies revealed that TFEB is a partner protein of SHP in upregulating autophagy/

lipolysis network genes (Fig 6). We, therefore, further determined the functional importance of TFEB in FGF19-mediated lipophagy and lipid-lowering effects in HT29 cells. In FGF19-treated cells, co-localization of LC3 puncta with the lipid droplet protein, PLIN2, was increased, and overexpression of TFEB substantially increased their co-localization, whereas downregulation of TFEB decreased it (Fig 7A), indicating that TFEB is required for FGF19-mediated lipophagy.

Downregulation of TFEB decreased the LC3 II/I ratio and increased p62 levels, whereas overexpression of TFEB led to the opposite effects, even in the presence of the lysosomal inhibitor bafilomycin A1 (Fig 7B), suggesting that TFEB increases the autophagic flux. Both pre-mRNA and protein levels of p62 were initially increased after overexpression of TFEB after FGF19 treatment (Appendix Fig S6A and B), which is consistent with the report that p62 is a target of TFEB (Settembre *et al*, 2011; Pan *et al*, 2020), but the p62 levels were decreased later times because of autophagic activation. Furthermore, downregulation of TFEB resulted in decreased expression of ULK1 and ATGL (Fig 7C). Consistent with these results, cellular TG and ApoB48 levels in FGF19-treated intestinal cells increased after TFEB downregulation (Fig 7D and E). These results, together, demonstrate that TFEB is a key activator of FGF19-mediated lipophagy, reducing intestinal TG and ApoB48 levels in HT29 cells.

Nuclear localization of TFEB is increased by feeding-induced FGF15 signaling in mouse intestine

The function of TFEB is regulated mainly by nuclear translocation (Puertollano *et al*, 2018; Di Malta *et al*, 2019). To understand the transcription activation mechanisms of intestinal autophagy/lipophagy genes by TFEB, we examined the effect of feeding on nuclear localization of TFEB in both liver and intestine. Nuclear levels of hepatic TFEB were substantially decreased in the fed mice, but intriguingly, the opposite was observed in the intestines of the same mice (Fig 8A). In contrast, feeding induced nuclear localization of SHP in both the liver and intestine (Fig 8A). Importantly, increased nuclear levels of TFEB and SHP and autophagic activation in the late fed-state were largely absent in FGF15-KO mice (Fig 8B–D), suggesting that feeding-induced endogenous FGF15 is critical for nuclear localization of both TFEB and SHP and autophagic activation in mouse intestine.

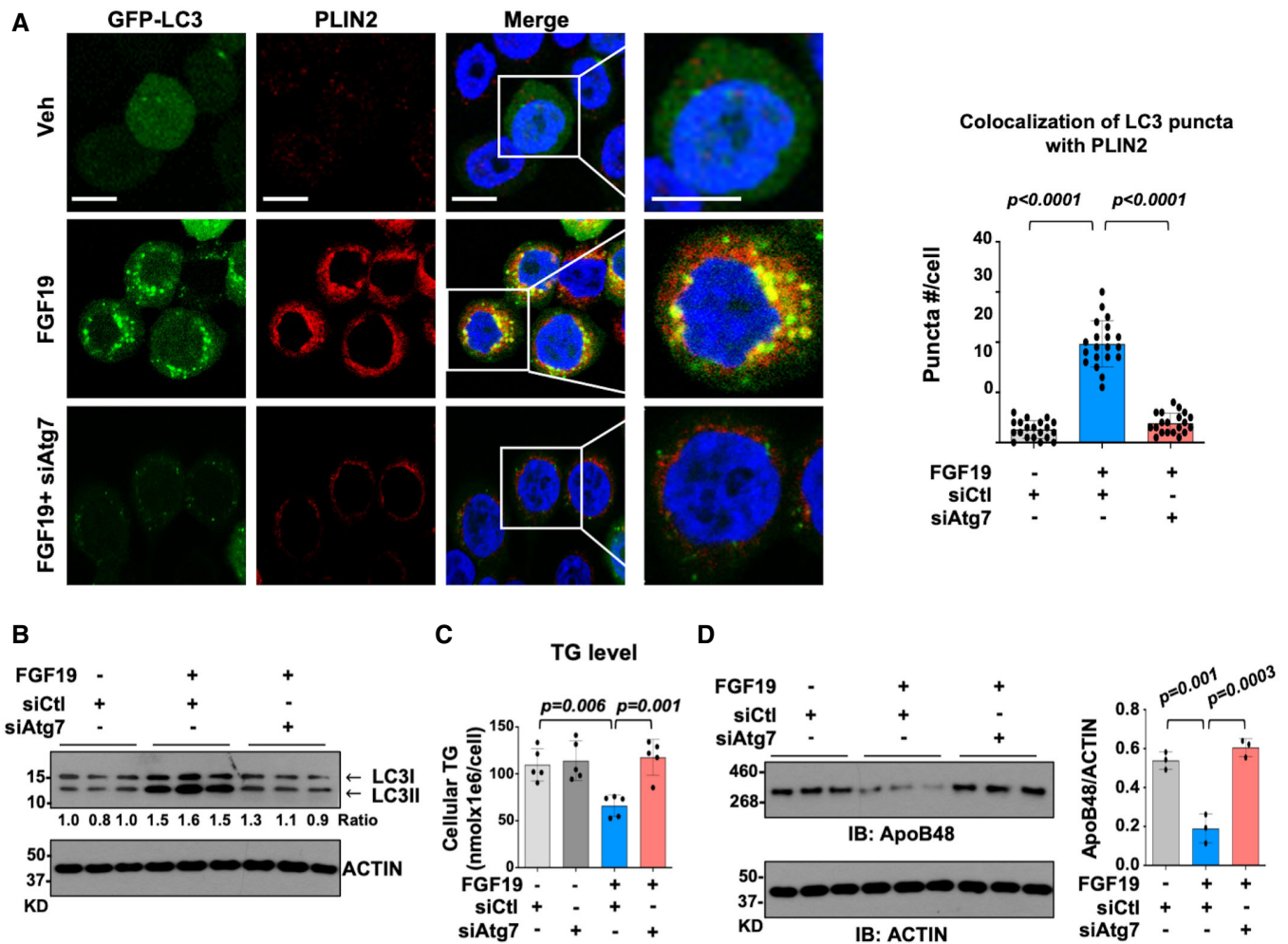


Figure 5. In HT29 cells, FGF19 activates lipophagy in a manner dependent on SHP, and FGF19 reduces TG and ApoB48 levels via lipophagy.

A HT29 cells were transfected with GFP-LC3 and with Atg7 siRNA or control scrambled RNA (siCtl) and incubated in serum-free medium containing 200 μ M oleic acid for 6 h followed by treatment with 50 ng/ml FGF19 for 6 h as described in Materials and Methods. The control group (Veh) was treated with vehicle for FGF19 and control siRNA. The FGF19 groups were treated with Atg7 siRNA or scrambled siRNA as indicated. Cells were imaged by confocal microscopy (Zeiss, LSM700). GFP-LC3 puncta were counted and the number of puncta/cell is shown at right ($n = 20$). Scale bar, 20 μ m.

B HT29 cells were transfected with Atg7 siRNA or control scrambled siRNA and 48 h later were treated with 50 ng/ml FGF19 for 12 h. LC3 and actin levels in cell extracts determined by IB ($n = 3$ culture plates).

C, D HT29 cells were transfected with Atg7 siRNA or control scrambled siRNA (siCtl) for 48 h and then treated with oleic acid for 6 h followed by treatment with 50 ng/ml FGF19 for 12 h. (C) Levels of TG in cell extracts ($n = 5$ culture plates). (D) ApoB48 and actin levels in cell extracts determined by IB. Bands were quantified and the LC3-II/LC3-I ratio is shown at the right ($n = 3$ culture plates).

Data information: (A–D) The mean and SD are plotted. Statistical significance was determined by one-way ANOVA with the Tukey post-test. P -values are indicated.

Feeding-induced FGF15/19 signaling increases nuclear localization of TFEB and SHP via PKC-mediated phosphorylation

Previous studies showed that FGF15/19 signaling inhibits nuclear localization of TFEB by mTOR/ERK-mediated phosphorylation at S211 in hepatocytes (Wang *et al*, 2020). Conversely, TFEB nuclear translocation is increased by PKC β -mediated phosphorylation of multiple C-terminal serines, including S461 and S462, in osteoclasts (Ferron *et al*, 2013). Nuclear localization of SHP is increased by FGF15/19-activated PKC ζ via T55 phosphorylation (Seok *et al*, 2013; Kim *et al*, 2018a, 2018b, 2020). PKC β is also activated in response to FGF19 treatment in hepatocytes (Appendix Fig S7A).

We, therefore, examined the potential role of these kinases in FGF19-induced nuclear localization of TFEB and SHP in mouse intestine and HT29 cells.

FGF19 treatment increased levels of the active phosphorylated forms of PKC β and PKC ζ , but not those of S6K, a direct mTOR target, and ERK in HT29 cells (Fig 8E). In temporal feeding experiments in C57BL/6 mice, both PKC β and PKC ζ were also activated by 3 h after feeding (Appendix Fig S7B), but activation of these kinases was largely absent in FGF15-KO mice (Fig 8F). Notably, levels of phosphorylated S6K, an mTOR downstream target, increased relatively earlier, 1–2 h after feeding, and returned to the basal levels by 3 h in control mice but remained elevated in FGF15-

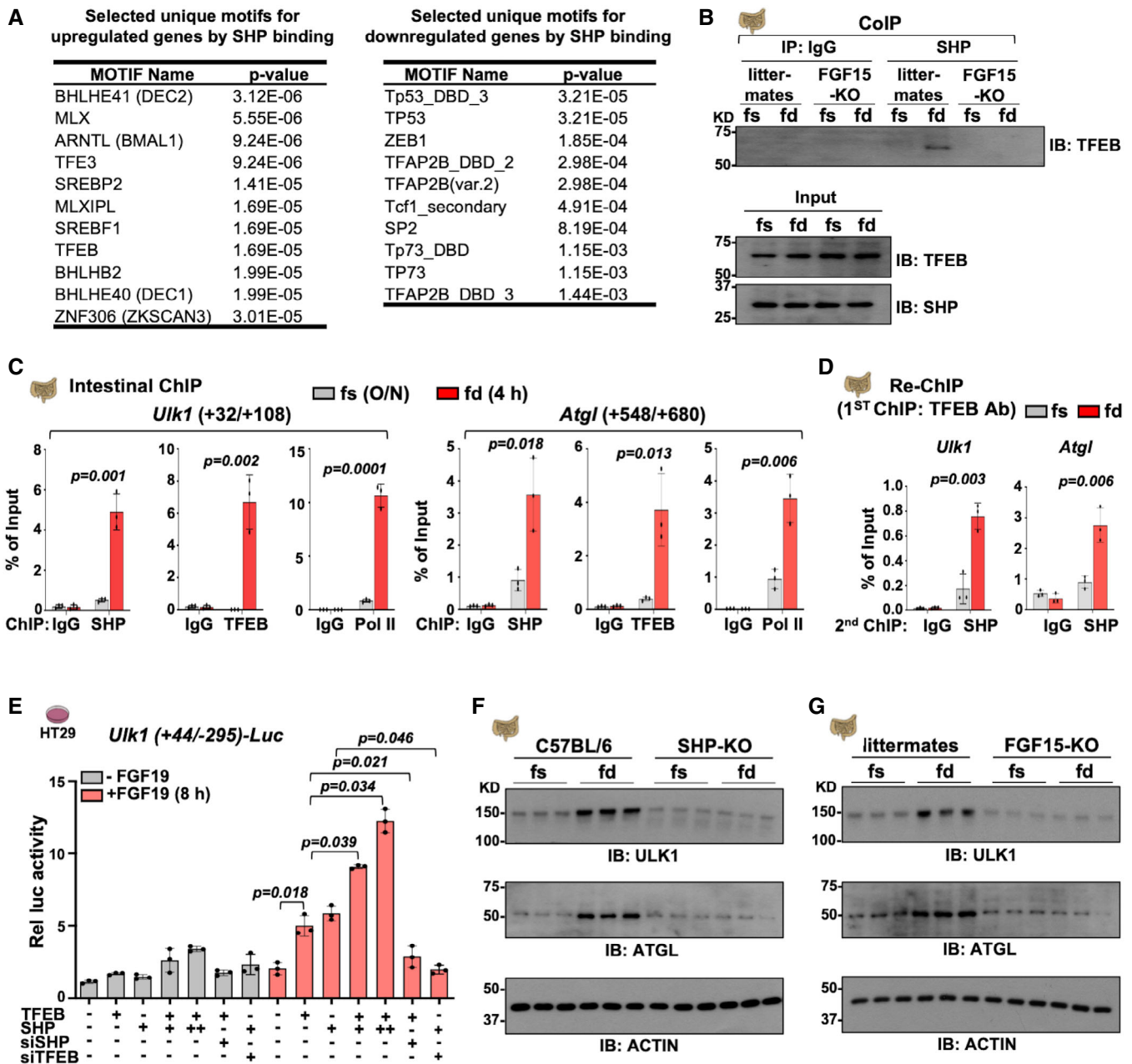


Figure 6. TFEB partners with SHP in the transcriptional induction of *Ulk1* and *Atgl*.

A Transcription factor binding motifs were identified *de novo* with MEME-ChIP analysis. Selected unique motifs within SHP binding peak regions for intestinal genes upregulated and downregulated by SHP binding are shown.

B–D Mice were re-fed for 2 h (B) or 4 h (C, D) after fasting overnight. (B) CoIP of TFEB with SHP. Upper panel: Levels of TFEB detected by IB in SHP and IgG immunoprecipitated samples. Lower panel: levels of TFEB and SHP in input samples detected by IB. Similar results were obtained in a second experiment. (C) Binding of the indicated factors at intestinal *Ulk1* determined by ChIP ($n = 3$ mice). (D) Co-occupancy of TFEB and SHP at *Ulk1* and *Atgl* determined by re-ChIP ($n = 3$ mice).

E HT29 cells were transfected with siRNA for *Shp* and/or *Tfeb* and then, 24 h later, further transfected with indicated plasmids for 24 h, and the cells were treated with FGF19 (50 ng/ml) for 8 h. Luciferase activities normalized to β -galactosidase activity are plotted ($n = 3$ culture plates).

F, G Protein levels detected by IB of ULK1 and ATGL in intestinal extracts from (F) C57BL/6 and SHP-KO mice or (G) FGF15-KO mice or littermates re-fed for 6 h after fasting overnight ($n = 3$ mice).

Data information: (C–E) The mean and SD are plotted. Statistical significance was determined by (C, D) two-way ANOVA with the Tukey post-test or (E) one-way ANOVA with the Tukey post-test. *P*-values are indicated.

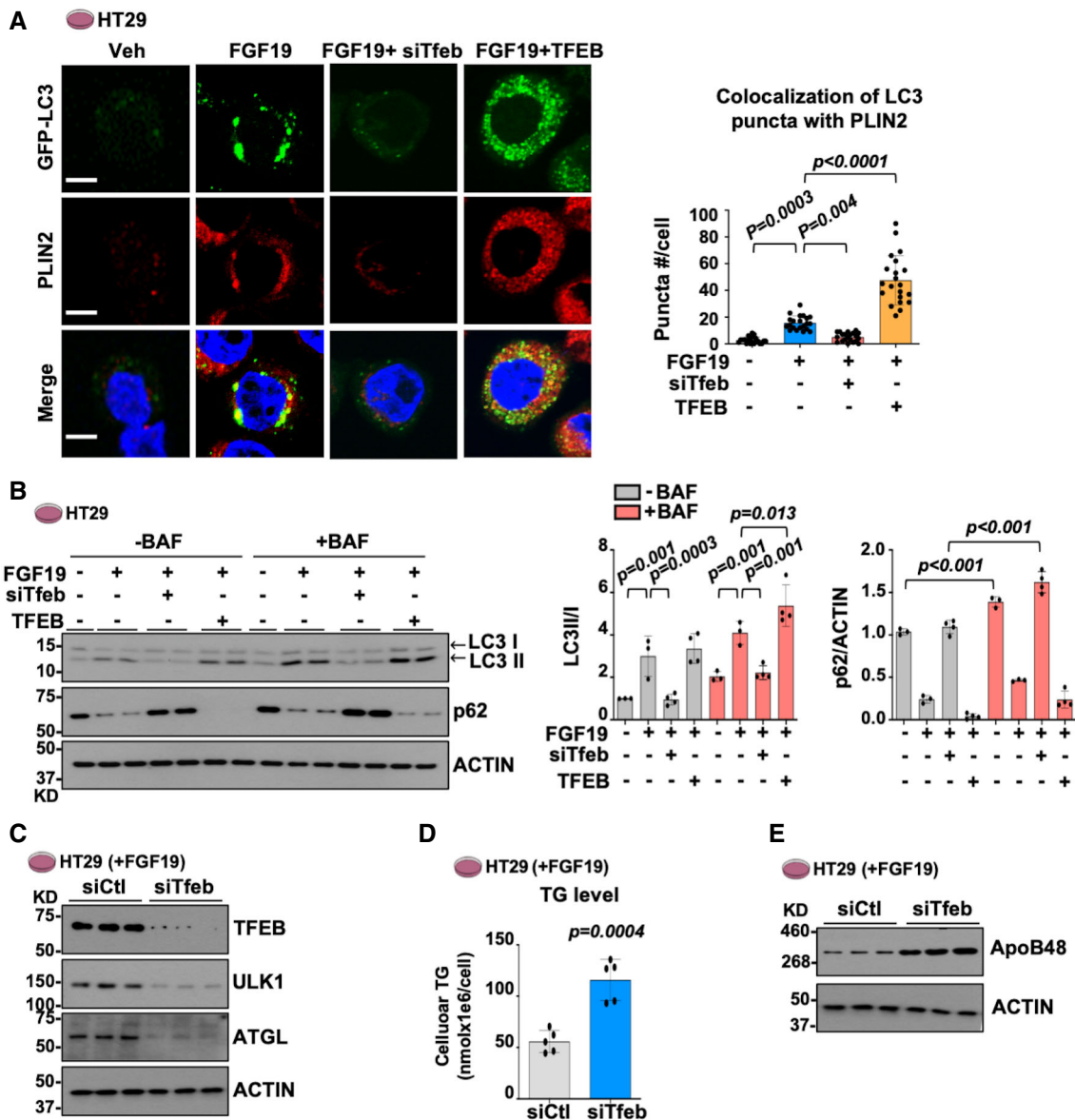


Figure 7. TFEB is critical for FGF19-mediated lipophagic activation and decreased TG levels in HT29 cells.

A HT29 cells were transfected with GFP-LC3 and with *Tfeb* siRNA or *Tfeb* expression plasmids and incubated in serum-free medium containing 200 μ M oleic acid for 6 h followed by treatment with 50 ng/ml FGF19 for 6 h as described in Materials and Methods. The control group (Veh) was treated with vehicle for FGF19 and transfected with control plasmid DNA and scrambled siRNA. The FGF19 groups were treated with control DNA or TFEB expression plasmid with *Tfeb* siRNA or scrambled siRNA as indicated. Cells were imaged by confocal microscopy (Zeiss, LSM700). GFP-LC3 puncta were counted and the number of puncta/cell is shown at right ($n = 20$ cells). Scale bar, 10 μ m.

B HT29 cells were transfected with siRNA for *Tfeb* (siTFEB) or control scrambled siRNA (siCtl), followed 48 h later by treatment with FGF19 or vehicle with or without 100 nM bafilomycin A1 (BAF) for 12 h. Levels of the indicated proteins determined by IB. LC3 II/I and p62/actin ratios are shown at the right ($n = 3-4$ culture plates).

C HT29 cells were transfected with siRNA for TFEB (siTFEB) or control RNA (siCtl), followed 48 h later by treatment with FGF19 or vehicle for 12 h. Protein levels detected by IB of ULK1 and ATGL ($n = 3$ culture plates).

D HT29 cells were treated with 50 ng/ml FGF19 for 12 h. Levels of triglycerides (TG) in cell extracts ($n = 5$ culture plates).

E HT29 cells were transfected with siRNA for *Tfeb* (siTFEB) or scrambled siRNA (siCtl), followed 48 h later by treatment with FGF19 or vehicle for 12 h. ApoB48 and actin levels in cell extracts determined by IB ($n = 3$ culture plates).

Data information: (A, B, D) The mean and SD are plotted. Statistical significance was determined by (A) one-way ANOVA with the Tukey post-test, (B) two-way ANOVA with the Tukey post-test, or (D) two-tailed Student's *t*-tests. *P*-values are indicated.

KO mice (Fig 8F), suggesting that feeding-induced endogenous FGF15 signaling might decrease mTOR activity in the late fed-state. In C57BL6 mice, autophagic activation determined by the LC3-II/I

ratio and p62, and LAMP1 levels were modestly increased as early as 1 h after feeding and substantially further enhanced 3 or 6 h after feeding (Appendix Fig S7C).

The FGF19-induced increase in nuclear levels of TFEB and autophagy in HT29 cells were blocked by treatment with inhibitors of PKC ζ or PKC β , which was blocked by inhibition of PKC ζ (Appendix Fig S8). The FGF19-mediated effects on increased TFEB

nuclear levels and autophagic activation were substantially diminished by the mutation in TFEB of S461A/S462A or deletion of the C-terminal 15 amino acids, whereas these FGF19 effects were still observed with the S211A or S142A mutants (Fig 8C, Appendix Fig

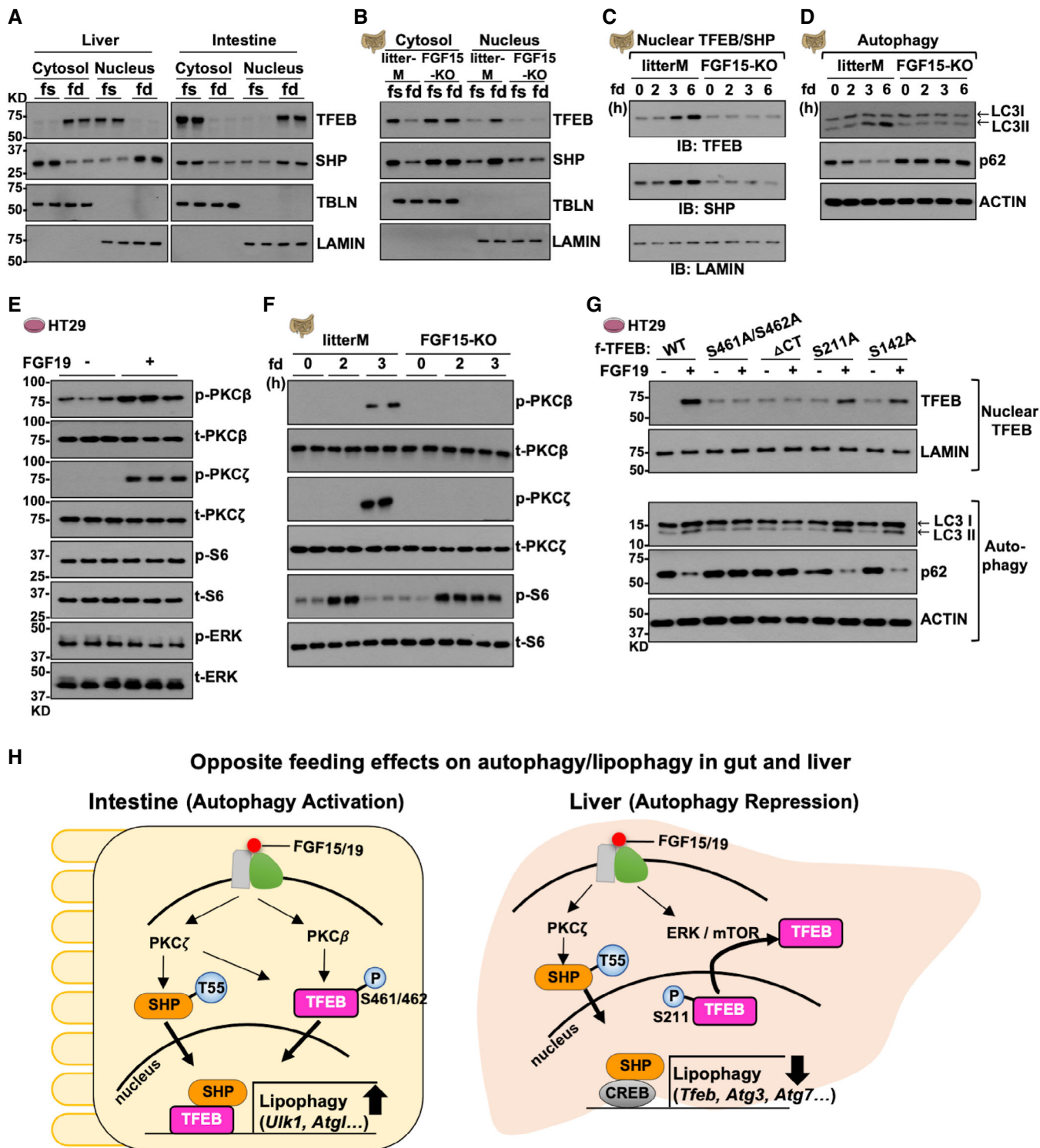


Figure 8.

Figure 8. Feeding-induced FGF15/19 signaling increases nuclear localization of both TFEB and SHP via PKC-mediated phosphorylation in mouse intestine and HT29 cells.

- A, B C57BL/6 (A) and FGF15-KO mice or littermates (B) were re-fed for 6 h after fasting overnight. The cytosolic and nuclear fractions were isolated from intestine or liver, and the indicated proteins were detected by IB ($n = 2$ mice). TBLN indicates tubulin.
- C, D FGF15-KO mice or littermates were fasted overnight and re-fed for the indicated times. (C) The nuclear fraction was isolated and the nuclear levels of TFEB, SHP, and LAMIN were determined by IB. (D) Levels of LC3, p62, and actin in cell extracts were determined by IB.
- E HT29 cells were cultured overnight in serum-free media and treated with vehicle or 50 ng/ml FGF19 for 30 min. The indicated proteins were detected by IB ($n = 3$ culture plates).
- F FGF15-KO mice or littermates were re-fed for 0, 2, or 3 h after fasting overnight. The indicated proteins in intestinal extracts were detected by IB ($n = 2$ mice).
- G HT29 cells were transfected with expression plasmids for flag-tagged TFEB or its mutants as indicated and 24 h later, cells were treated with FGF19 (50 ng/ml) for 12 h. Δ CT indicates the TFEB mutant with a C-terminal deletion of 15 amino acids. The indicated proteins were detected by IB ($n = 3$ culture plates).
- H Model of the opposite feeding regulation of autophagy in liver and intestine. Feeding activates intestinal lipophagy, paradoxically in the nutrient-rich fed conditions, limiting postprandial TG levels. Mechanistically, in mouse intestine and intestinal cells, postprandial FGF15/19 signaling increases nuclear translocation of both TFEB and SHP via PKC β / ζ -mediated phosphorylation at S461/S462 in TFEB and PKC ζ -mediated phosphorylation at T55 in SHP, leading to transcription activation of autophagy genes, *Ulk1* and *Atg1*, in the late fed-state. In contrast, in the liver, in response to feeding-induced FGF15/19 signaling, TFEB is exported to the cytoplasm via mTOR/ERK-mediated phosphorylation at S211 and SHP is translocated into the nucleus via PKC ζ -mediated T55 phosphorylation, leading to transcription repression of autophagy network genes, including *Tfeb*, *Atg3*, and *Atg7*.

S9A and B). Notably, FGF19 treatment increased phosphorylated Ser levels in TFEB WT, but not in the TFEB S461A/S462A or the C-terminal deletion mutant (Appendix Fig S9C). Increased autophagy after FGF19 treatment was also largely absent with the T55A SHP mutant (Appendix Fig S9D). These data, together, indicate that FGF19 signaling activates PKC β / ζ in intestinal cells, resulting in phosphorylation of TFEB at S461/S462 and SHP at T55 and nuclear localization of both TFEB and SHP for induction of the lipophagy network genes.

Collectively, these results from mechanistic studies in mouse intestine and HT29 cells demonstrate that feeding-induced FGF15/19 signaling activates the gene-activating functions of both TFEB and SHP via increasing their nuclear levels, which involves PKC β / ζ -mediated phosphorylation, leading to transcription induction of the TFEB/SHP targets, *Ulk1* and *Atg1*.

Discussion

Autophagy is generally thought to be activated under nutrient-deprived conditions and repressed after feeding. A previous seminal study has shown that macroautophagy is activated after 24 h of fasting in most tissues in mice, including liver, heart, muscle, kidney, and exocrine pancreas, although autophagic responses to fasting are not equal among tissues (Mizushima et al, 2004). In this paper, we report that, surprisingly, feeding activates intestinal autophagy via FGF15/19 signal-activated SHP and TFEB, which is contrary to the usual activation of autophagy under nutrient deprivation and its repression under nutrient-rich conditions. Remarkably, feeding regulation of autophagy is tissue-specific, with activation in the intestine and inhibition in the liver. Consistent with these opposite effects, postprandial FGF15/19 signaling increases nuclear localization of the key autophagic activator TFEB in the intestine, while decreasing it in the liver. FGF15/19 signaling increases nuclear localization of SHP in both tissues, so that SHP acts in a tissue-specific manner as a repressor of autophagy genes in the liver and as an activation partner with TFEB of autophagy genes in the intestine.

By comparing the intestinal SHP ChIP-seq data with the transcriptome data (Kim et al, 2018a), we show that lipid absorption/synthesis and bile acid recycling genes contain SHP binding sites and are likely repressed by SHP binding. These results are consistent

with the known functions of SHP as a corepressor. Unexpectedly, however, SHP binding peaks were also detected at genes that are activated by SHP binding, including autophagy, lipid catabolism, and circadian network genes. Remarkably, global motif analyses revealed motifs for different sets of transcription factors at genes activated or repressed by SHP binding. In this study, we show that after feeding, SHP partners with TFEB to upregulate intestinal *Ulk1* and *Atg1*, which are essential for autophagy/lipophagy (Sathyanarayan et al, 2017; Schulze et al, 2017; Zechner et al, 2017). Furthermore, in HT29 cells, FGF19 activates intestinal lipophagy, detected by co-localization of LC3 puncta with the lipid droplet protein PLIN2, and this activation was dependent on both SHP and TFEB. Our genomic analyses suggest that SHP functions as a coactivator of intestinal TFEB, but additional structural and molecular biochemical analyses will be needed to firmly establish this novel coactivator mechanism.

The transcription function of TFEB is regulated mainly by subcellular localization. As a shuttling protein between the lysosomal surface, the cytoplasm, and the nucleus, TFEB export from the nucleus is mediated by mTOR/ERK-dependent phosphorylation under nutrient-rich conditions (Settembre et al, 2012; Napolitano et al, 2018; Puertollano et al, 2018). Conversely, TFEB stability and nuclear localization are increased by PKC β -mediated phosphorylation at multiple Ser residues in the C-terminus (Ferron et al, 2013). In hepatocytes, TFEB nuclear localization is inhibited by FGF15/19-activated mTOR/ERK via phosphorylation of S211, resulting in inhibition of bile acid synthesis (Wang et al, 2020). Interestingly, in the present study utilizing FGF15-KO mice, we observed that feeding-induced endogenous FGF15 signaling activated both PKC β and PKC ζ and increased nuclear levels of TFEB in mouse intestine. Consistent with these findings, in HT29 cells, FGF19 treatment did not activate mTOR or ERK, but instead, activated PKC β and PKC ζ , leading to phosphorylation of TFEB at S461/S462 and increased nuclear localization of TFEB and increased autophagic activation.

Based on these findings, we propose the following model (Fig 8H). In the intestine, feeding-induced FGF15/19 signaling activates PKC β and PKC ζ , resulting in phosphorylation of TFEB at S461/S462 and that of SHP at T55. These post-translational events lead to increased nuclear localization of both TFEB and SHP and consequently, increased co-occupancy of these proteins at *Ulk1* and *Atg1*, resulting in transcriptional activation of lipophagy genes. In

contrast, in the liver, TFEB is phosphorylated at S211 via FGF15/19-activated mTOR/ERK and translocated to the cytoplasm (Wang *et al.*, 2020), and SHP is phosphorylated at T55 by PKC ζ and translocated into the nucleus, resulting in repression of CREB-target autophagy genes as shown previously (Byun *et al.*, 2017). It is intriguing that feeding-induced FGF15/19 signaling activates different sets of kinases in the liver and intestine, resulting in phosphorylation of TFEB at different residues for the opposite effects on TFEB nuclear translocation. Furthermore, global motif analyses for SHP binding sites in mouse intestine from the current study and the published ChIP-seq (Kim *et al.*, 2015) and autophagy studies in mouse liver (Byun *et al.*, 2017) revealed that FGF15/19-activated SHP interacts with different sets of transcription factors in the gut and liver, for example, activating TFEB to promote gut autophagy, while inhibiting CREB to repress hepatic autophagy.

Our findings suggest that feeding activation of intestinal autophagy likely involves both post-translational and transcriptional mechanisms. mTOR was activated 1–2 h after feeding in mouse intestine (Fig 7E and F) at the same time as the initial feeding activation of gut autophagy was observed. These findings were surprising as mTOR is a well-known repressor of autophagy via direct phosphorylation of ULK1 at Ser-757, disrupting the ULK1 and AMPK interaction under nutrient-rich conditions (Kim *et al.*, 2011). It is not clear whether the increased intestinal autophagy at 1–2 h is directly mediated by mTOR, but it is possible that intestinal mTOR may activate autophagy early after feeding via phosphorylation of ULK1 at residues other than Ser-757 or phosphorylation of other proteins involved in autophagic pathway. Given that mTOR activation correlated with the increased LC3 II/I ratio and decreased p62 levels in mice, intestinal autophagy is acutely activated early after feeding via mTOR-mediated post-translational mechanisms. In contrast, FGF15/19 signal-activated SHP and TFEB may sustain the activation by providing a continuous supply of proteins involved in lysosomal biogenesis, autophagy, and lipolysis pathways in the late fed-state via transcriptional induction of lipophagy network genes.

An essential function of the gut is to distribute dietary lipids via TG-rich chylomicrons throughout the body. Paradoxical feeding activation of gut lipophagy identified in this study, thus, may be physiologically relevant by preventing excess TGs available for secretion. In SHP-KO and FGF15-KO mice, feeding activation of intestinal autophagy was not observed, and levels of postprandial TG and ApoB48, the intestinal marker of chylomicrons, were elevated. Consistent with our findings, a previous study has demonstrated that SHP mediates diurnal regulation of microsomal triglyceride transfer protein (MTP), a key protein for lipoprotein assembly, and that TG levels in ApoB-lipoprotein particles are elevated in SHP-KO mice in a circadian manner (Pan *et al.*, 2010; Hussain, 2014). Notably, our genomic analyses in mouse intestine revealed that SHP directly upregulates circadian genes, including *Bmal* and *Nampt*, key diurnal regulators of metabolism. In addition, plasma FGF15 levels are diurnal (Katafuchi *et al.*, 2015), and TFEB also mediates rhythmic induction of autophagy genes (Pastore *et al.*, 2019). Circadian physiology may, thus, play an important role in feeding induction of gut lipophagy by FGF15/19-activated SHP and TFEB.

In conclusion, we demonstrate that paradoxically in the nutrient-rich fed-state, FGF15/19 signal-activated SHP and TFEB promote transcriptional induction of intestinal lipophagy, regulating postprandial TGs and ApoB48-containing chylomicron levels available

for secretion. As elevated postprandial lipids can cause dyslipidemia and obesity, the intestinal FGF15/19-SHP-TFEB pathway that reduces postprandial lipids via lipophagic activation may provide novel targets for treating obesity-related metabolic disorders.

Materials and Methods

Antibodies and reagents

Information on antibodies and antibody dilutions are provided in Appendix Table S5 and materials and reagents used in this study are provided in Appendix Table S6.

Mice

Eight- to twelve-week-old male mice SHP-KO (Wang *et al.*, 2002) with C57BL/6 mice as WT controls and FGF15-KO (Kong *et al.*, 2014) or littermates were used. For fasting/feeding experiments, mice were fasted overnight (12–16 h) and then, re-fed for 1–6 h with normal chow (Teklad, 8664, Madison, WI). All animal experiments were approved by the Institutional Animal Care and Use Committees of the University of Illinois at Urbana-Champaign (UIUC).

Intestinal SHP ChIP-seq

Mice were fasted overnight for 12 h and then, re-fed for 4 h with normal chow (Teklad, 8664, Madison, WI) and the jejunum and ileum of intestines were collected for ChIP assay using SHP antibody. Three independent sets of input and immunoprecipitated samples were analyzed and each set contained samples pooled from three mice. Eighteen ng of DNA was used for genomic sequencing using the Illumina/Solexa Genome Analyzer II (Biotechnology Center, UIUC). ChIP-seq data were analyzed using the AQUAS TF and histone ChIP-seq pipeline and mapped to the mouse reference genome (UCSC mm10) using bwa. ChIP-seq peaks were identified by MACS followed by IDR (Irreproducible Discovery Rate). Optimal peaks with an IDR value < 0.05 were kept. To estimate the coverage of our data, the Pearson's correlation coefficient was calculated for sub-sampled data and the full dataset using bigwigCorrelate from deepTools (version 1.5.11). To determine the quality of the ChIP-seq data, quality metrics from the ENCODE project were used as benchmarks. The heatmap plot around the ChIP-seq peak center was generated using computeMartix and plotHeatmap from the deepTools package. We performed ChIP-seq using SHP antibody (Santa Cruz Biotech, sc-30169) and confirmed SHP binding at selected genes using a mixture of SHP antibodies (Santa Cruz Biotech, sc-30169 and Abcam, ab96605) (Figs 2E and 3E) or the Abcam antibody alone (Appendix Fig S4).

Comparative genomic analyses

For the comparison of the intestinal SHP cistrome with transcriptome analysis, published intestinal RNA-seq data from C57BL/6 wild type (WT) and SHP-KO mice (Kim *et al.*, 2018a) were used. The differential expression profiles of RNA-seq, analyzed by the edgeR-based R, version 3.5.0 (R Core Development Team, Vienna, Austria) pipeline, were presented as a MA plot showing ratio intensity. For all comparisons, $P < 0.05$ was considered significant.

G/O analysis

The subsets of differentially expressed genes detected by RNA-seq that also contained SHP binding peaks in the ChIP-seq analysis were subjected to G/O analysis using the DAVID program, version 6.8 (Leidos Biomedical Research, Frederick, MD).

DNA Motif analysis

Transcription factor motifs in SHP binding regions (± 100 bp from the center of the peaks) were identified *de novo* with MEME-ChIP. Motifs with E-values < 0.05 with lengths ranging from 6 to 15 were compared to known motifs in database JASPAR_CORE_2020.

Histological analysis

For mouse studies, intestinal tissues were embedded in paraffin for IHC. As previously described (Byun *et al.*, 2020), LC3 and ApoB48 in paraffin sections were detected using the HRP/DAB (ABC) detection IHC kit (Abcam, ab64261), and nuclei were stained with hematoxylin. Tissue sectioning was done at the histopathology laboratory at the University of Illinois at Urbana-Champaign and the stained samples were imaged with NanoZoomer (Hamamatsu).

Lipophagy study in HT29 cells

HT29 human intestinal cells (ATCC, HTB-38) were cultured in Dulbecco's modified Eagle's medium with 10% fetal bovine serum on coverslips for two days, transfected with siRNA for *Shp*, *Atg7*, *Tfeb* or control scrambled RNA, and 24 h later, transfected with GFP-LC3 expression plasmids (2 μ g) and control plasmid DNA, *Shp*, or *Tfeb* expression plasmids (2 μ g). Twenty-four hours later, the cells were incubated in serum-free medium containing 200 μ M oleic acid (O3008, Sigma) for 6 h followed by further treatment with 50 ng/ml FGF19 or vehicle for 6 h. After fixation with 4% formaldehyde for 15 min, cells were permeabilized by incubation in 0.5% Triton-X100/PBS for 15 min. Cells were incubated with primary PLIN2 antibody (dilution 1:100 in PBS) overnight at 4°C and then with Alexa 647 goat anti-guinea pig IgG (dilution 1:500 in PBS) for 1 h at room temperature, and counterstained with DAPI. Nuclei were labeled by Hoechst staining (dilution 1:1,000) for 5 min and then, washed with PBS three times. In a second set of experiments using BODIPY staining, the cells were incubated in serum-free medium containing 400 μ M oleic acid for 6 h followed by further treatment with FGF19 for 12 h. After fixation with 4% formaldehyde for 15 min, cells were permeabilized by incubation in 0.5% Triton-X100/PBS for 15 min. The cells were incubated with 1 μ g/ml of BODIPY (D-3861, Life Technologies) in 150 mM NaCl for 10 min, washed with PBS, and counterstained with DAPI. Nuclei were labeled by Hoechst staining for 5 min and then, washed with PBS three times. Cells were imaged by confocal microscopy (Zeiss, LSM700).

Measurement of TG levels

TG levels in mouse intestines (Sigma, TR0100) and in HT29 intestinal cells (Abcam, ab65336) were measured according to the manufacturers' protocols.

ChIP and re-ChIP

Mouse intestines were minced, washed twice with PBS, and incubated with 1% (w/v) formaldehyde for 10 min and with 125 mM glycine for 5 min, and ChIP was performed as described previously (Kim *et al.*, 2018a). Briefly, chromatin samples were sonicated and incubated with 2 μ g antibody or control IgG overnight at 4°C and then with a Protein G Sepharose containing salmon-sperm DNA for 1 h. The slurry was washed three times with 0.1% SDS, 1% Triton X-100, 2 mM EDTA, 20 mM Tris-HCl, pH 8.0 containing successively 150 mM NaCl, 500 mM NaCl, and 0.25 M LiCl, and then, incubated overnight at 65°C to reverse the crosslinking. For re-ChIP, immunoprecipitated chromatin was eluted by incubation with 10 mM DTT for 30 min at 37°C, the eluate was diluted 20-fold and re-precipitated, and crosslinks were reversed. DNA was isolated and quantified by qPCR. Primers are shown in Appendix Table S7A.

Immunoblotting (IB)

Mouse intestine and liver tissues, and cells were washed with ice-cold PBS and homogenized in RIPA buffer (50 mM Tris-HCl pH 7.4, 150 mM NaCl, 1% Triton X-100, 1 mM EDTA pH 8.0, 0.1% SDS, 1 mM DTT) containing protease and phosphatase inhibitors (1 mM PMSF, 1 mg/ml Aprotinin, 1 mg/ml Leupeptin, 2 μ M Pepstatin A, 1 mM NaF, 1 mM Na_3VO_4 , 0.4 μ M Na_2MoO_4 , 0.5 μ M $\text{Na}_4\text{P}_2\text{O}_7$). Samples were incubated for 20 min at 4°C and centrifuged at 16,000 \times g for 10 min. Supernatants were subjected to electrophoresis, transferred to PVDF membranes, blocked in TBS-Tween 20 containing 5% non-fat milk for 1 h at room temperature, and incubated with primary antibodies overnight at 4°C, followed by secondary antibody at room temperature for 40 min. Band densities were quantified using ImageJ software.

Co-immunoprecipitation (CoIP)

Mouse intestines were finely chopped and washed in ice-cold PBS, resuspended in lysis buffer (50 mM Tris, pH 8.0, 150 mM NaCl, 2 mM EDTA, 0.3% Nonidet P40, 10% glycerol) and homogenized. Then, samples were incubated for 20 min at 4°C and centrifuged at 16,000 \times g for 10 min. The supernatants were incubated overnight with 1 μ g of antibodies, and then with 35 μ l of 25% protein G agarose. Two hours later, agarose beads were washed with the CoIP buffer three times and bound proteins were detected by IB.

Nuclear/cytoplasmic fractionation

HT29 intestinal cells were transfected with expression plasmids, flag-TFEB WT, flag-SHP, or mutants (Settembre *et al.*, 2011; Ferron *et al.*, 2013; Wang *et al.*, 2020) and 1 day later, cells were treated with FGF19 (50 ng/ml) for 12 h. Mouse intestine and liver tissues and HT29 cells were resuspended in hypotonic buffer containing 10 mM HEPES (pH 8.0), 10 mM KCl, 1 mM EDTA, 1 mM DTT, and protease and phosphatase inhibitors for 15 min on ice, and then, 10% NP40 was added to a final concentration of 0.2% and the lysate was homogenized and centrifuged at 4,000 \times g for 3 min at 4°C. The supernatant was saved as the cytosolic fraction. The pellet was resuspended in buffer containing 20 mM HEPES, 0.4 M NaCl, 1–2 mM EDTA, and protease and phosphatase inhibitors, and vortexed twice for 20 min at

4°C. After centrifugation at 14,000 g for 10 min, the resulting supernatant was saved as the nuclear fraction. The quality of fractionation was monitored by levels of lamin and tubulin.

Luciferase reporter assay

Genomic DNA fragments containing the *Ulk1* promoter (+44 to –295) were inserted into the pGL3-luc plasmid (Promega, Inc). HT29 cells were transfected with 200 ng reporter plasmids, 100 ng of β -gal plasmids, 5–50 ng expression plasmids. For SHP downregulation studies, cells were transfected with siRNA and then, 24 h later, the cells were transfected with reporter and expression plasmids for 24 h, and then, treated with FGF19 (50 ng/ml) for 8 h. Luciferase activities were normalized to β -galactosidase activities.

RT-qPCR

Intestinal total RNAs were isolated using the RNeasy Kit (Qiagen, Valencia, CA), cDNA was synthesized, and mRNA and pre-mRNA levels were determined by RT-qPCR with the iCycler iQ. The amount of mRNA for each gene was normalized to those of *36b4* mRNA. Sequences of primers are in Appendix Table S7B.

Experimental design and statistics

At least three mice or cell culture plates per experimental group (biological replicates) were analyzed based on expected variability and to provide statistical analysis. No randomization or blinding techniques were used, and no data were excluded. GraphPad Prism 9 was used for data analysis. Statistical significance was determined by the Student's two-tailed *t*-test or one- or two-way ANOVA with the Tukey post-test for single or multiple comparisons as appropriate.

Data availability

The primary RNA-seq data reported previously (Kim *et al*, 2018a) and the primary intestinal ChIP-Seq data for SHP from this study have been deposited in the NCBI GEO database with the accession numbers, GSE126939 (<https://www.ncbi.nlm.nih.gov/geo/query/acc.cgi?acc=GSE126939>) and GSE197549 (<https://www.ncbi.nlm.nih.gov/geo/query/acc.cgi?acc=GSE197549>), respectively.

Expanded View for this article is available online.

Acknowledgements

We thank H. Eric Xu at Van Andel Research Institute for providing recombinant FGF19. We also thank Carmine Settembre at Telethon Institute of Genetics & Medicine, Tiangang Li at University of Oklahoma, Mathieu Ferron at University of Montreal, and Gerard Karsenty at Columbia University, for providing TFEB expression plasmids. This study was supported by an American Heart Association Scientist Development Award (16SDG27570006) to Y-CK and by R01 grants from the National Institutes of Health (DK062777 and DK095842) to JKK.

Author contributions

Sunmi Seok: Conceptualization; Data curation; Formal analysis; Investigation; Writing—original draft; Writing—review & editing. **Young-Chae Kim:** Conceptualization; Formal analysis; Investigation; Writing—original draft; Writing—

review & editing. **Yang Zhang:** Formal analysis. **Bo Kong:** Resources. **Grace Guo:** Resources. **Jian Ma:** Formal analysis. **Byron Kemper:** Formal analysis; Writing—original draft; Writing—review & editing. **Jongsook Kim Kemper:** Conceptualization; Formal analysis; Supervision; Funding acquisition; Writing—original draft; Project administration; Writing—review & editing.

In addition to the CRediT author contributions listed above, the contributions in detail are:

SS, Y-CK, and JKK designed research; SS and Y-CK performed experiments; Y-CK, YZ, and JM performed genomic analyses; BoK and GG provided key materials; SS, Y-CK, and ByK analyzed data; and SS, Y-CK, ByK, and JKK wrote the paper.

Disclosure and competing interests statement

The authors declare that they have no conflict of interest.

References

- Baek SH, Kim KI (2017) Epigenetic control of autophagy: nuclear events gain more attention. *Mol Cell* 65: 781–785
- Byun S, Kim D-H, Ryerson D, Kim Y-C, Sun H, Kong BO, Yau P, Guo G, Xu HE, Kemper B *et al* (2018) Postprandial FGF19-induced phosphorylation by Src is critical for FXR function in bile acid homeostasis. *Nat Commun* 9: 2590
- Byun S, Kim YC, Zhang Y, Kong B, Guo G, Sadoshima J, Ma J, Kemper B, Kemper JK (2017) A postprandial FGF19-SHP-LSD1 regulatory axis mediates epigenetic repression of hepatic autophagy. *EMBO J* 36: 1755–1769
- Byun S, Seok S, Kim YC, Zhang Y, Yau P, Iwamori N, Xu HE, Ma J, Kemper B, Kemper JK (2020) Fasting-induced FGF21 signaling activates hepatic autophagy and lipid degradation via JMJD3 histone demethylase. *Nat Commun* 11: 807
- Chauhan S, Goodwin JG, Chauhan S, Manyam G, Wang J, Kamat AM, Boyd DD (2013) ZKSCAN3 is a master transcriptional repressor of autophagy. *Mol Cell* 50: 16–28
- Di Malta C, Cinque L, Settembre C (2019) Transcriptional regulation of autophagy: mechanisms and diseases. *Front Cell Dev Biol* 7: 114
- Ferron M, Settembre C, Shimazu J, Lacombe J, Kato S, Rawlings DJ, Ballabio A, Karsenty G (2013) A RANKL-PKC β -TFEB signaling cascade is necessary for lysosomal biogenesis in osteoclasts. *Genes Dev* 27: 955–969
- Fullgrabe J, Klionsky DJ, Joseph B (2014) The return of the nucleus: transcriptional and epigenetic control of autophagy. *Nat Rev Mol Cell Biol* 15: 65–74
- Gadaleta RM, Moschetta A (2019) Metabolic Messengers: fibroblast growth factor 15/19. *Nat Metab* 1: 588–594
- He C, Klionsky DJ (2009) Regulation mechanisms and signaling pathways of autophagy. *Annu Rev Genet* 43: 67–93
- Hodson L, Gunn PJ (2019) The regulation of hepatic fatty acid synthesis and partitioning: the effect of nutritional state. *Nat Rev Endocrinol* 15: 689–700
- Hussain MM (2014) Intestinal lipid absorption and lipoprotein formation. *Curr Opin Lipidol* 25: 200–206
- Katafuchi T, Esterhazy D, Lemoff A, Ding X, Sondhi V, Kliewer SA, Mirzaei H, Mangelsdorf DJ (2015) Detection of FGF15 in plasma by stable isotope standards and capture by anti-peptide antibodies and targeted mass spectrometry. *Cell Metab* 21: 898–904
- Kerr TA, Saeki S, Schneider M, Schaefer K, Berdy S, Redder T, Shan B, Russell DW, Schwarz M (2002) Loss of nuclear receptor SHP impairs but does not eliminate negative feedback regulation of bile acid synthesis. *Dev Cell* 2: 713–720

- Kim J, Kundu M, Viollet B, Guan KL (2011) AMPK and mTOR regulate autophagy through direct phosphorylation of Ulk1. *Nat Cell Biol* 13: 132–141
- Kim YC, Byun S, Zhang Y, Seok S, Kemper B, Ma J, Kemper JK (2015) Liver CHIP-seq analysis in FGF19-treated mice reveals SHP as a global transcriptional partner of SREBP-2. *Genome Biol* 16: 268
- Kim YC, Byun S, Seok S, Guo G, Xu HE, Kemper B, Kemper JK (2018a) Small heterodimer partner and fibroblast growth factor 19 inhibit expression of NPC1L1 in mouse intestine and cholesterol absorption. *Gastroenterology* 156: 1052–1065
- Kim YC, Seok S, Byun S, Kong B, Zhang Y, Guo G, Xie W, Ma J, Kemper B, Kemper JK (2018b) AhR and SHP regulate phosphatidylcholine and S-adenosylmethionine levels in the one-carbon cycle. *Nat Commun* 9: 540
- Kim Y, Seok S, Zhang Y, Ma J, Kong B, Guo G, Kemper B, Kemper JK (2020) Intestinal FGF15/19 physiologically repress hepatic lipogenesis in the late fed-state by activating SHP and DNMT3A. *Nat Commun* 11: 5969
- Kliwer SA, Mangelsdorf DJ (2015) Bile acids as hormones: the FXR-FGF15/19 pathway. *Dig Dis* 33: 327–331
- Klionsky DJ, Abdel-Aziz AK, Abdelfatah S, Abdellatif M, Abdoli A, Abel S, Abeliovich H, Abildgaard MH, Abudu YP, Acevedo-Arozena A et al (2021) Guidelines for the use and interpretation of assays for monitoring autophagy (4th edition)(1). *Autophagy* 17: 1–382
- Kong BO, Huang J, Zhu Y, Li G, Williams J, Shen S, Aleksunes LM, Richardson JR, Apte U, Rudnick DA et al (2014) Fibroblast growth factor 15 deficiency impairs liver regeneration in mice. *Am J Physiol Gastrointest Liver Physiol* 306: G893–G902
- Kounakis K, Chaniotakis M, Markaki M, Tavernarakis N (2019) Emerging roles of lipophagy in health and disease. *Front Cell Dev Biol* 7: 185
- Kuma A, Hatano M, Matsui M, Yamamoto A, Nakaya H, Yoshimori T, Ohsumi Y, Tokuhisa T, Mizushima N (2004) The role of autophagy during the early neonatal starvation period. *Nature* 432: 1032–1036
- Lee J, Padhye A, Sharma A, Song G, Miao J, Mo YY, Wang L, Kemper JK (2010) A pathway involving farnesoid X receptor and small heterodimer partner positively regulates hepatic sirtuin 1 levels via microRNA-34a inhibition. *J Biol Chem* 285: 12604–12611
- Lee JM, Wagner M, Xiao R, Kim KH, Feng D, Lazar MA, Moore DD (2014) Nutrient-sensing nuclear receptors coordinate autophagy. *Nature* 516: 112–115
- Lee Y, Moore DD (2002) Dual mechanism for repression of the monomeric orphan receptor liver receptor homologous protein-1 (LRH-1) by the orphan small heterodimer partner (SHP). *J Biol Chem* 277: 2463–2467
- Levine B, Klionsky DJ (2004) Development by self-digestion: molecular mechanisms and biological functions of autophagy. *Dev Cell* 6: 463–477
- Martinez-Lopez N, Singh R (2015) Autophagy and lipid droplets in the liver. *Annu Rev Nutr* 35: 215–237
- Miao J, Xiao Z, Kanamaluru D, Min G, Yau PM, Veenstra TD, Ellis E, Strom S, Suino-Powell K, Xu HE et al (2009) Bile acid signaling pathways increase stability of Small Heterodimer Partner (SHP) by inhibiting ubiquitin-proteasomal degradation. *Genes Dev* 23: 986–996
- Mizushima N, Yamamoto A, Matsui M, Yoshimori T, Ohsumi Y (2004) *In vivo* analysis of autophagy in response to nutrient starvation using transgenic mice expressing a fluorescent autophagosome marker. *Mol Biol Cell* 15: 1101–1111
- Morishita H, Mizushima N (2019) Diverse cellular roles of autophagy. *Annu Rev Cell Dev Biol* 35: 453–475
- Napolitano G, Esposito A, Choi H, Matarese M, Benedetti V, Di Malta C, Monfregola J, Medina DL, Lippincott-Schwartz J, Ballabio A (2018) mTOR-dependent phosphorylation controls TFEB nuclear export. *Nat Commun* 9: 3312
- Nguyen JT, Riessen R, Zhang T, Kieffer C, Anakk S (2021) Deletion of intestinal SHP impairs short-term response to cholic acid challenge in male mice. *Endocrinology* 162: bqab063
- Pan BO, Li J, Parajuli N, Tian Z, Wu P, Lewno MT, Zou J, Wang W, Bedford L, Mayer RJ et al (2020) The calcineurin-TFEB-p62 pathway mediates the activation of cardiac macroautophagy by proteasomal malfunction. *Circ Res* 127: 502–518
- Pan X, Zhang Y, Wang L, Hussain MM (2010) Diurnal regulation of MTP and plasma triglyceride by CLOCK is mediated by SHP. *Cell Metab* 12: 174–186
- Pastore N, Vainshtein A, Herz NJ, Huynh T, Brunetti L, Klisch TJ, Mutarelli M, Annunziata P, Kinouchi K, Brunetti-Pierri N et al (2019) Nutrient-sensitive transcription factors TFEB and TFE3 couple autophagy and metabolism to the peripheral clock. *EMBO J* 38: e101347
- Phillips ML, Pullinger C, Kroes I, Kroes J, Hardman DA, Chen G, Curtiss LK, Gutierrez MM, Kane JP, Schumaker VN (1997) A single copy of apolipoprotein B-48 is present on the human chylomicron remnant. *J Lipid Res* 38: 1170–1177
- Puertollano R, Ferguson SM, Brugarolas J, Ballabio A (2018) The complex relationship between TFEB transcription factor phosphorylation and subcellular localization. *EMBO J* 37: e98804
- Sathyanarayan A, Mashek MT, Mashek DG (2017) ATGL promotes autophagy/lipophagy via SIRT1 to control hepatic lipid droplet catabolism. *Cell Rep* 19: 1–9
- Schulze RJ, Sathyanarayan A, Mashek DG (2017) Breaking fat: the regulation and mechanisms of lipophagy. *Biochim Biophys Acta Mol Cell Biol Lipids* 1862: 1178–1187
- Seok S, Fu T, Choi S-E, Li Y, Zhu R, Kumar S, Sun X, Yoon G, Kang Y, Zhong W et al (2014) Transcriptional regulation of autophagy by an FXR-CREB axis. *Nature* 516: 108–111
- Seok S, Kanamaluru D, Xiao Z, Ryerson D, Choi SE, Suino-Powell K, Xu HE, Veenstra TD, Kemper JK (2013) Bile acid signal-induced phosphorylation of small heterodimer partner by protein kinase Czeta is critical for epigenomic regulation of liver metabolic genes. *J Biol Chem* 288: 23252–23263
- Seok S, Kim YC, Byun S, Choi S, Xiao Z, Iwamori N, Zhang Y, Wang C, Ma J, Ge K et al (2018) Fasting-induced JMJD3 histone demethylase epigenetically activates mitochondrial fatty acid beta-oxidation. *J Clin Invest* 128: 3144–3159
- Seol W, Choi H, Moore DD (1996) An orphan nuclear hormone receptor that lacks a DNA binding domain and heterodimerizes with other receptors. *Science* 272: 1336–1339
- Settembre C, Ballabio A (2014) Cell metabolism: autophagy transcribed. *Nature* 516: 40–41
- Settembre C, De Cegli R, Mansueto G, Saha PK, Vetrini F, Visvikis O, Huynh T, Carissimo A, Palmer D, Jürgen Klisch T et al (2013) TFEB controls cellular lipid metabolism through a starvation-induced autoregulatory loop. *Nat Cell Biol* 15: 647–658
- Settembre C, Di Malta C, Polito VA, Arcibibia MG, Vetrini F, Erdin S, Erdin SU, Huynh T, Medina D, Colella P et al (2011) TFEB links autophagy to lysosomal biogenesis. *Science* 332: 1429–1433
- Settembre C, Zoncu R, Medina DL, Vetrini F, Erdin S, Erdin S, Huynh T, Ferron M, Karsenty G, Vellard MC et al (2012) A lysosome-to-nucleus signalling mechanism senses and regulates the lysosome via mTOR and TFEB. *EMBO J* 31: 1095–1108
- Singh R, Kaushik S, Wang Y, Xiang Y, Novak I, Komatsu M, Tanaka K, Cuervo AM, Czaja MJ (2009) Autophagy regulates lipid metabolism. *Nature* 458: 1131–1135
- Tsai TH, Chen E, Li L, Saha P, Lee HJ, Huang LS, Shelness GS, Chan L, Chang BH (2017) The constitutive lipid droplet protein PLIN2 regulates autophagy in liver. *Autophagy* 13: 1130–1144

Wang LI, Lee Y-K, Bundman D, Han Y, Thevananther S, Kim C-S, Chua SS, Wei P, Heyman RA, Karin M *et al* (2002) Redundant pathways for negative feedback regulation of bile acid production. *Dev Cell* 2: 721–731

Wang Y, Gunewardena S, Li F, Matye DJ, Chen C, Chao X, Jung T, Zhang Y, Czerwiński M, Ni H-M *et al* (2020) An FGF15/19-TFEB regulatory loop controls hepatic cholesterol and bile acid homeostasis. *Nat Commun* 11: 3612

Zechner R, Madeo F, Kratky D (2017) Cytosolic lipolysis and lipophagy: two sides of the same coin. *Nat Rev Mol Cell Biol* 18: 671–684

Zhang P, Csaki LS, Ronquillo E, Baufeld LJ, Lin JY, Gutierrez A, Dwyer JR, Brindley DN, Fong LG, Tontonoz P *et al* (2019) Lipin 2/3 phosphatidic acid phosphatases maintain phospholipid homeostasis to regulate chylomicron synthesis. *J Clin Invest* 129: 281–295



License: This is an open access article under the terms of the Creative Commons Attribution-NonCommercial-NoDerivs License, which permits use and distribution in any medium, provided the original work is properly cited, the use is non-commercial and no modifications or adaptations are made.